Journal of *Marine Science and Engineering*

MDPI

Article

Improved Velocity Estimation Method for Doppler Sonar Based on Accuracy Evaluation and Selection

Yongshou Yang and Shiliang Fang *

Key Laboratory of Underwater Acoustic Signal Processing, Ministry of Education, Southeast University, Nanjing 210096, China; ysyang@seu.edu.cn
* Correspondence: slfang@seu.edu.cn

Abstract: The matched filtering method and the waveform-tracking method cannot maintain optimal velocity estimation performance all of the time. In order to solve this problem, this paper proposes an improved velocity estimation method for Doppler sonar, based on accuracy evaluation and selection. The echo of Doppler sonar is divided into several segments with the same width as the transmitted pulse, and each segment is regarded as the echo of the corresponding water layer. According to our study's results, the velocity estimation accuracy of each segment is positively correlated with the ratio of its autocorrelation modulus to its power. Based on this conclusion, a velocity accuracy criterion with high accuracy and low complexity is designed in order to select the optimal velocity estimation for water layers or bottoms. The proposed accuracy selection method flexibly selects the echo interval to be processed according to the accuracy criterion, so as to maintain the optimal estimation of the current's or bottom's velocity. Water tank and field experiments using a prototype Doppler sonar device demonstrates that, compared with the matched filtering method and the waveform-tracking method, the average velocity estimation accuracy and bias of the proposed method are superior.

Keywords: velocity estimation; accuracy estimation; accuracy criterion; Doppler shift; Doppler sonar

Citation: Yang, Y.; Fang, S. Improved Velocity Estimation Method for Doppler Sonar Based on Accuracy Evaluation and Selection. *J. Mar. Sci. Eng.* **2021**, *9*, 576. https://doi.org/10.3390/jmse9060576

Academic Editor: Philippe Blondel

Received: 17 April 2021
Accepted: 23 May 2021
Published: 26 May 2021

1. Introduction

Doppler sonar is a popular acoustic technique used for measuring water velocity and profile discharge in natural and man-made waterways. Due to its advantages of high estimation accuracy, multiple measurement parameters, and low measurement costs, Doppler sonar has been widely used in the fields of hydrological surveying, water resource exploration, underwater protection and navigation [1–4], etc. Since narrowband technology gradually took shape in the 1970s, the acoustic Doppler measurement technology has experienced more than 50 years of development and application. The measurement methods used in Doppler sonar include the pulse-to-pulse incoherent method [5], the pulse-to-pulse coherent method [6], and the broadband method [7].

The incoherent method is suitable for applications where the detection range and velocity measurement range are large, while high stratification and velocity measurement accuracy are not required. The coherent method has high range and velocity resolution, but has the shortcoming of range–velocity ambiguity [8,9]; it is suitable for shallow water applications with thin layer thickness, where high velocity measurement accuracy is required. The broadband method combines the advantages of the incoherent and coherent methods, while its range and velocity resolution no longer restrict one another [10]. Phase-encoding technology enables the improvement of the broadband method's velocity estimation accuracy while maintaining its velocity measurement range and detection range [11]. The broadband method has obvious advantages, and has become the most popular choice.

The accuracy of velocity estimation directly determines the performance of velocity distribution estimation, profile discharge measurement, or underwater navigation in the measurement applications of Doppler sonar [12]; therefore, velocity estimation accuracy is

the core performance parameter of Doppler sonar. The factors that affect the accuracy of velocity estimation are as follows:

(1) Code autocorrelation characteristics: Broadband Doppler sonar uses a phase-encoded signal as the transmitted signal, and requires the code to have a narrow autocorrelation peak and low peak sidelobe level (PSL) in order to obtain as many statistically independent samples as possible in a small scattering area. Codes with non-ideal characteristics will reduce the independence of echo samples, increase the influence of self-noise, and decrease velocity estimation accuracy [13]. The Barker code is the code known to be closest to the ideal characteristics.

(2) Number of code repeats: The purpose of transmitting phase-encoded signals repeatedly in broadband Doppler sonar is to maximize the energy transmitted into the water and increase the signal-to-noise ratio (SNR) of the echoes. This repetition will cause additional echo autocorrelation peaks, and reduce the independence of echo samples [14]; however, the repetition also reduces the proportion of the echo segment that produces self-noise in the total echo, and decreases the influence of self-noise. When the transmitted pulse width is constant, a greater number of code repeats leads to a smaller velocity estimation error, and a larger velocity measurement range.

(3) Beam spreading: The single beam of Doppler sonar can only measure the radial component of the velocity vector of scatterers. When the moving scatterers pass through the beam-illuminated area, beam spreading will cause the Doppler shift to extend in a certain range [15]. In other words, Doppler sonar receives a series of different frequency shifts instead of a constant Doppler shift. The wider the beam, the larger the range of the Doppler shifts, and the greater the velocity estimation error.

(4) Correlation delay and ambiguity velocity: Doppler sonar estimates Doppler shift by measuring the change of the echo phase in correlation delay. Regardless of the velocity ambiguity, correlation delay determines the velocity measurement range. The shorter the correlation delay, the larger the velocity measurement range; however, as the velocity measurement range increases, the sensitivity of the sonar system to the velocity change decreases, which in turn leads to a decline in the velocity estimation accuracy [16]; therefore, it is important to choose an appropriate ambiguity velocity, according to the target velocity. In some improved Doppler sonar systems, the estimated velocity of the current ping is used to dynamically adjust the ambiguity velocity of the next ping, in order to maintain optimal measurement sensitivity.

(5) Length of observation time: The correlation between adjacent samples of sonar echo significantly affects the velocity estimation accuracy. As the observation time increases, the scatterers in the beam-illuminated area will change significantly, and the correlation between adjacent echo samples will become weaker [17]. If the expected current velocity is small, a longer observation time can be selected; otherwise, a shorter observation time can be selected.

(6) Environmental factors: These factors include velocity distribution and environmental noise. Acoustic Doppler measurement is based on the assumption that the scatterers in the water move in a constant and uniform manner. If this assumption is invalid, the velocity estimation accuracy will decrease. If the water is turbulent, the scatterers within a given depth cell move with multiple radial velocity components, and the correlation of echoes and the velocity estimation accuracy will be reduced.

Research on velocity estimation performance has always been the focus in the field of acoustic Doppler measurement. The bias error in moving-boat Doppler sonar current measurement can be divided into two categories: calibration error, and application error. Major sources of calibration error and the influence of parameters on the discharge uncertainty were analyzed in [18]. Aurélien Despax et al. studied the uncertainty of Doppler sonar discharge measurement caused by cross-section selection and human operation by using repeated measures experiments, and put forward some strategies to reduce measurement uncertainty [19]. Doppler sonar is usually installed on a moving boat for measurement. The authors of [20,21] proposed a method to improve velocity estimation accuracy by

compensating for the boat's motion. Fractional Fourier transform was used to separate the component of strong scatterers from the Doppler sonar echo, and to improve the accuracy and stability of water velocity estimation [22]. Transmitted pulse distortion caused by the nonlinear effect significantly affected velocity estimation accuracy. The fundamental signal and second harmonic signal were used to estimate the velocity and reduce the velocity estimation error caused by the nonlinear effect [23]. The authors of [24] pointed out that the measurement deviation of the phase-encoded signal is mainly determined by the energy of the autocorrelation function of a single baseband pulse (SBPAF), and gave a calculation method for the coding phase through which the SBPAF achieves maximum energy. A waveform design method for a dual-band, coherent, phase-encoded transmitted signal—by dividing the signal spectrum into two—was proposed in [25]. This method enriches the form of the transmitted signal of the Doppler sonar.

Doppler sonar usually divides the echo into multiple segments with the same width as the transmitted pulse, and each segment contains the information of the corresponding water layer. The Doppler shift of each segment is estimated in order to obtain the current velocity of the corresponding layer. Due to the superposition of scattering echoes from adjacent layers and the time-varying SNR, the velocity estimation of existing methods cannot be kept optimal. The existing bottom velocity measurement methods include the matched filtering (MF) method and the waveform-tracking (WT) method. The MF method first locates the bottom echo interval according to the matched filtering result, and then estimates the Doppler shift of the echo in the interval as the bottom velocity. The upper limit of the output SNR of the matched filter only depends on the energy of the input signal, and is independent of the type of waveform [26]. A high matched filtering result does not guarantee optimal velocity estimation accuracy. The WT method first locates the bottom echo interval according to the signal envelope, and then estimates the Doppler shift of the echo in the interval as the bottom velocity. Theoretically, the bottom echo consists of the anterior transition zone (ATZ), the posterior transition zone (PTZ), and the stability zone (SZ). Only the part of the echo in the transition zone comes from the scattering of the water bottom; thereby, the velocity estimation error of the transition zone is relatively larger than that of the SZ. The ATZ and PTZ are removed in some improved methods, and only the SZ is retained for Doppler estimation. However, the transition zone's width is affected by several factors, and it deviates greatly from the theoretical calculation. Meanwhile, due to the beam angle, Doppler shift, and beam spreading, the bottom echo width varies greatly between samples; therefore, it is difficult to improve the estimation accuracy of the bottom velocity by removing the transition zone from the bottom echo. In summary, the existing MF and WT methods find it difficult to maintain optimal velocity estimation.

In order to overcome the shortcomings of the existing methods, a velocity estimation method based on accuracy evaluation and selection is proposed in this paper. In Section 2, based on the relationship between velocity estimation accuracy and the echo autocorrelation function, an accuracy selection method for optimal velocity measurement is proposed. In Section 3, water tank and field experiments are conducted with a prototype Doppler sonar device. The experimental results demonstrate the correctness and practicability of the proposed method. Finally, Section 4 highlights the conclusions of this study.

2. Methods

The autocorrelation functions of narrowband and broadband echoes are studied in Section 2.1 in order to provide a theoretical basis. In Section 2.2, the relationship between velocity estimation accuracy and the echo autocorrelation function is studied, and a criterion and an accuracy selection method for optimal velocity measurement are proposed.

2.1. Autocorrelation Function of Sonar Echo

The main transmitted signals in acoustic Doppler measurement are narrowband continuous wave pulses and broadband phase-encoded pulses. The following is a study on their autocorrelation function.

2.1.1. Narrowband Case

Assuming the underwater scatterer moves towards the Doppler sonar with a constant radial velocity v, the distance function between the scatterer and the Doppler sonar is $r(t)$ can be expressed as:

$$r(t) = r_0 - vt \tag{1}$$

where r_0 is the distance between the scatterer and the Doppler sonar at $t = 0$. Assuming the transmitted signal of Doppler sonar is the continuous wave pulse $x(t)$, and its expression is:

$$x(t) = A\cos(\omega_c t) \tag{2}$$

where A is the signal amplitude and ω_c is the carrier frequency, scatterer echo $y(t)$ can be expressed as a time delay function of the transmitted signal:

$$y(t) = x\left(t - \frac{2r(t)}{c}\right) \tag{3}$$

where c is the underwater sound speed 1500 m/s. Equation (3) ignores the change in echo amplitude. Substitute Equations (1) and (2) into Equation (3):

$$y(t) = A\cos\left(\omega_c t + \frac{4\pi v}{\lambda}t - \frac{4\pi r_0}{\lambda}\right) \tag{4}$$

where λ is the wavelength of the sound wave. The sonar receiver performs orthogonal demodulation and echo filtering, and shifts the Doppler spectrum to baseband. A pair of orthogonal signals obtained after down-conversion is expressed as complex forms:

$$y_c(t) = \frac{A}{2}\exp\left[-j2\pi\left(\frac{2v}{\lambda}t - \frac{2r_0}{\lambda}\right)\right] \tag{5}$$

The complex autocorrelation function $R(\tau)$ is defined as:

$$R(\tau) = \frac{1}{T-\tau}\int_0^{T-\tau} y_c(t+\tau)y_c^*(t)dt, \quad \tau \geq 0 \tag{6}$$

where T is the width of the transmitted pulse, and τ is the autocorrelation delay. Incorporate Equation (5) into Equation (6) to get the complex autocorrelation function of the narrowband echo after simplification:

$$R(\tau) = \frac{A^2}{4}\exp(-j\omega_d\tau) \tag{7}$$

where $\omega_d = 4\pi v/\lambda$, and represents the Doppler shift caused by the relative movement between the scatterers and the sonar. Equation (7) demonstrates that the complex autocorrelation function of narrowband echo is only related to the correlation delay τ and the Doppler shift ω_d, and is independent of the carrier frequency ω_c and the initial phase of the echo.

2.1.2. Broadband Case

Phase-encoded signals are among the commonly transmitted signals of broadband Doppler sonar. Here, a binary phase-encoded signal is used as an example from which to derive the autocorrelation function of the broadband echo. Suppose the expression of a phase-encoded transmitted signal $x(t)$ is:

$$x(t) = \sum_{n=0}^{N-1} x_n(t) \tag{8}$$

where N is the number of chips in the transmitted signal, and $x_n(t)$ represents the nth chip, which can be expressed as:

$$x_n(t) = A\cos(\omega_c t + \varphi_n)w_n(t) \tag{9}$$

where A is the signal amplitude, φ_n is the initial carrier phase of the nth symbol, $w_n(t) = u(t - nT_c) - u(t - nT_c - T_c)$ is the time window function, T_c is the chip width, and $u(t)$ is the unit step function. Equations (8) and (9) can be substituted into Equation (3) in order to obtain the expression of the broadband echo signal:

$$y(t) = A\sum_{n=0}^{N-1}\cos\left(\omega_c t - \frac{4\pi r(t)}{\lambda} + \varphi_n\right)w_n\left(t - \frac{2r(t)}{c}\right) \tag{10}$$

Similarly to in the narrowband case, a pair of orthogonal signals is obtained after down-conversion, which is expressed in complex forms:

$$y_c(t) \approx \frac{A}{2}\exp\left(-j\frac{4\pi r(t)}{\lambda}\right)\sum_{n=0}^{N-1}\exp(j\varphi_n)w_n\left(t - \frac{2r_0}{c}\right) \tag{11}$$

Only the window function part is approximated in Equation (11), ignoring the expansion or contraction of the echo. Since the scatterer speed is much smaller than the underwater sound speed ($v \ll c$), the ratio of the pulse width change caused by the Doppler effect to the original width is $2v/c$, which can be ignored. By incorporating Equation (11) into Equation (6), the complex autocorrelation function of the broadband echo is obtained after simplification:

$$R(\tau) = \frac{A^2}{4(T-\tau)}\exp(j\omega_d\tau)\int_0^{T-\tau}\left[\sum_{n=0}^{N-2}\exp(j\varphi_n)w_n(t+\tau)\right]\left[\sum_{m=0}^{N-2}\exp(j\varphi_m)w_m(t)\right]dt \tag{12}$$

where $T = NT_c$ represents the pulse width, and ω_d represents the Doppler shift caused by the scatterers' movement. When the chips are the same, and thus the signal is not encoded, the result of Equation (12) is the same as that of the narrowband case. For the phase-encoded signal, the integral terms of Equation (12) represent the autocorrelation of the code, and the integral result is only related to the chip width T_c and the correlation delay τ. Taking 4-times-repeated 7-bit Barker code as an example, the relationship between the integral term values in Equation (12) and the correlation delay τ is shown in Table 1. It should be noted that the correlation delay in the complex autocorrelation algorithm is generally an integer multiple of the code width.

Table 1. Relationship between the autocorrelation function amplitude and correlation delay of the broadband echo (Taking 4-times-repeated 7-bit Barker code as an example).

	Correlation Delay τ	**Integral Term**	**Amplitude of $R(\tau)$**
1	$7T_c$	$21T_c$	$A^2/4$
2	$14T_c$	$14T_c$	$A^2/4$
3	$21T_c$	$7T_c$	$A^2/4$

As in the narrowband case, the autocorrelation function phase of the broadband echo is only related to the correlation delay and the Doppler shift, and is independent of the carrier frequency and the initial phase of the echo. Compared with the narrowband signal, the autocorrelation function of the phase-encoded signal adds a fractional product term related to the code. The product term only affects the amplitude of the autocorrelation function, not its phase. The autocorrelation function amplitude of the phase-encoded signal is the same as that of the narrowband signal, especially when the correlation delay is an integer multiple of the code width.

2.2. Accuracy Selection Method

In order to overcome the shortcomings of existing methods, a velocity measurement method based on accuracy estimation and echo selection is proposed, which is called the accuracy selection method.

The principle of the accuracy selection method is as follows: Firstly, the interval of one water layer or bottom echo is extended to three times the width of the transmitted pulse. A sub-echo with the same width as the transmitted pulse is intercepted from the beginning of the extended interval, and its accuracy criterion value is calculated. The above processing is repeated by sliding, point by point, until the end of the extended interval. The Doppler shift of the sub-echo with the largest criterion value is selected in order to estimate the interested water layer or bottom velocity. Compared with the WT method, the accuracy selection method does not need to accurately locate the position of the bottom echo, and can overcome the influence of interference echo and time-varying SNR. Although the computational complexity is increased, the effect on the data update rate of Doppler sonar is negligible. The principles of the accuracy criterion and the accuracy selection method are introduced in detail below.

A velocity estimation accuracy criterion with high accuracy and low complexity is proposed. The value of this criterion is positively correlated with the velocity estimation accuracy. The larger the criterion value, the more accurate the velocity estimation of the echo. The criterion is used to select the sub-echo with the highest estimation accuracy from one layer or bottom echo. The detailed derivation process of the criterion is given below. The Doppler shift in acoustic current measurement is a random signal. Theoretically, the first and second moments of power spectral density (PSD) function can be used to estimate the mean and variance of the Doppler shift, under the condition that the Doppler spectrum has been shifted to the baseband. The expressions of the mean value $\overline{\omega}$ and variance σ_{ω}^2 of the Doppler shift estimated from the signal PSD are as follows:

$$\overline{\omega} = \frac{\int_{-\pi}^{\pi} \omega S(\omega) d\omega}{\int_{-\pi}^{\pi} S(\omega) d\omega} \tag{13}$$

$$\sigma_{\omega}^2 = \frac{\int_{-\pi}^{\pi} (\omega - \overline{\omega})^2 S(\omega) d\omega}{\int_{-\pi}^{\pi} S(\omega) d\omega} \tag{14}$$

where $S(\omega)$ is the PSD function of the sonar echo. By substituting Equation (13) into Equation (14), the estimated expression of the Doppler shift variance can be obtained:

$$\sigma_{\omega}^2 = \frac{\int_{-\pi}^{\pi} \omega^2 S(\omega) d\omega}{\int_{-\pi}^{\pi} S(\omega) d\omega} - \left[\frac{\int_{-\pi}^{\pi} \omega S(\omega) d\omega}{\int_{-\pi}^{\pi} S(\omega) d\omega} \right]^2 \tag{15}$$

Since the PSD method usually has a high computational complexity, and its noise suppression ability is weaker than that of the autocorrelation method, the autocorrelation function is often used to replace the PSD function for parameter estimation in practice. According to the Wiener–Khinchin theorem, the relationship between the autocorrelation function $R(\tau)$ and the PSD function is as follows:

$$R(\tau) = \frac{1}{2\pi} \int_{-\pi}^{\pi} S(\omega) e^{j\omega\tau} d\omega \tag{16}$$

where τ is the autocorrelation delay. The first and second derivatives of Equation (16) are obtained:

$$R'(\tau) = \frac{j}{2\pi} \int_{-\pi}^{\pi} \omega S_s(\omega) e^{j\omega\tau} d\omega \tag{17}$$

$$R''(\tau) = -\frac{1}{2\pi} \int_{-\pi}^{\pi} \omega^2 S_s(\omega) e^{j\omega\tau} d\omega \tag{18}$$

Let τ in Equations (16)–(18) be 0, and the relationship between three moments of the PSD function and the autocorrelation function can be obtained as follows:

$$\int_{-\pi}^{\pi} S(\omega)d\omega = 2\pi R(0) \tag{19}$$

$$\int_{-\pi}^{\pi} \omega S(\omega)d\omega = -\mathrm{j}2\pi R'(0) \tag{20}$$

$$\int_{-\pi}^{\pi} \omega^2 S(\omega)d\omega = -2\pi R''(0) \tag{21}$$

Equations (19)–(21) can be substituted into Equation (15) to get the following results:

$$\sigma_\omega^2 = -\frac{R''(0)}{R(0)} + \left[\frac{R'(0)}{R(0)}\right]^2 \tag{22}$$

The calculation formulae of the first and second derivatives of the autocorrelation function are derived below. The autocorrelation function needs to be expressed in the polar coordinate form, as shown in Equation (23). As shown in Section 2.1, the complex autocorrelation functions of the narrowband and broadband echoes of Doppler sonar can be expressed in polar coordinate form, so the assumption of Equation (23) is reasonable and correct:

$$R(\tau) = A(\tau)e^{\mathrm{j}\varphi(\tau)} \tag{23}$$

where $A(\tau)$ is the amplitude function and $\varphi(\tau)$ is the phase function. The first and second derivatives of Equation (23) are obtained as follows:

$$R'(\tau) = \left[A'(\tau) + \mathrm{j}A(\tau)\varphi'(\tau)\right]e^{\mathrm{j}\varphi(\tau)} \tag{24}$$

$$R''(\tau) = \left\{A''(\tau) + 2\mathrm{j}\varphi'(\tau)A'(\tau) + \left[\mathrm{j}\varphi''(\tau) - \left(\varphi'(\tau)\right)^2\right]A(\tau)\right\}e^{\mathrm{j}\varphi(\tau)} \tag{25}$$

The amplitude function $A(\tau)$ and the phase function $\varphi(\tau)$ are the real even function and the real odd function of τ, respectively. If $A(\tau)$ and $\varphi(\tau)$ are double differentiable at $\tau = 0$, then $A''(\tau)$ and $\varphi'(\tau)$ are even functions, and $A'(\tau)$ and $\varphi''(\tau)$ are odd functions. Therefore, $\varphi(0) = 0$, $A'(0) = 0$ and $\varphi''(0) = 0$ can be obtained. Let $\tau = 0$ in Equations (23–25) in order to obtain the following expressions:

$$R(0) = A(0) \tag{26}$$

$$R'(0) = \mathrm{j}A(0)\varphi'(0) \tag{27}$$

$$R''(0) = A''(0) - A(0)\left[\varphi'(0)\right]^2 \tag{28}$$

Equations (26–28) can be substituted into Equation (22) to get the following result:

$$\sigma_\omega^2 = -\frac{A''(0)}{A(0)} \tag{29}$$

Conducting Taylor expansion on $A(\tau)$ at $\tau = 0$ and taking the first three terms, the equation $A''(0) \approx 2[A(\tau) - A(0)]/\tau^2$ can be obtained. Substituting this equation into Equation (29), the following result is obtained:

$$\sigma_\omega^2 = \frac{2}{\tau^2}\left[1 - \frac{A(\tau)}{A(0)}\right] \tag{30}$$

According to Equation (23), $A(\tau) = |R(\tau)|$ and $A(0) = R(0)$. Substituting them into Equation (30), the variance σ_ω^2 can be expressed as follows:

$$\sigma_\omega^2 = \frac{2}{\tau^2}\left[1 - \frac{|R(\tau)|}{R(0)}\right] \tag{31}$$

Equation (31) is the final expression for estimating the frequency variance using the autocorrelation function, where $|R(\tau)|$ represents the modulus of $R(\tau)$, which can be regarded as an estimation of signal power. $R(0)$ is the total power of signal and noise. $|R(\tau)|/R(0)$ represents the ratio of signal power to echo power, which is inversely proportional to the frequency estimation error. $|R(\tau)|/R(0)$ is regarded as the criterion of Doppler shift estimation accuracy in this paper, which is called the η criterion. The larger the η criterion value, the smaller the variance of frequency estimation.

$$\eta = \frac{|R(\tau)|}{R(0)} \tag{32}$$

In this paper, the relationship between the η criterion value and velocity estimation accuracy is verified by the field data. The bottom echo data measured by Doppler sonar when the ship is stationary is taken as the analysis object, and the theoretical bottom velocity is zero. Figure 1 shows the relation curve between the η criterion value and the velocity estimation error of 160 sub-echoes. The thick and thin solid lines represent the η criterion curve and the velocity estimation error curve, respectively. The dotted line marks the location of the maximum η criterion value. The η criterion values in Figure 1 are largely inversely proportional to the velocity estimation error. The velocity estimation error at the position of the maximum η criterion value is almost the smallest, which is consistent with the theoretical prediction.

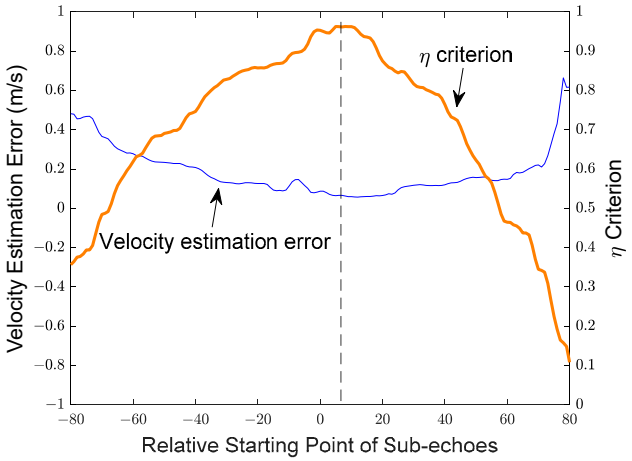

Figure 1. The η criterion value and the velocity estimation error calculated from the field data.

The flow chart of the accuracy selection method is shown in Figure 2. Firstly, the one-beam echo is divided into several echo segments with the same width as the transmitted pulse, and one segment is regarded as the echo of one water layer. Taking a segment as the center, a total of three segments nearby are selected as the extended echo of the current water layer. A time window with the same width as the transmitted pulse is used to intercept an echo from the beginning of the extended echo, which is called a sub-echo. Sliding the time window point by point until the end of the extended echo, multiple sub-echoes are intercepted in turn. The η criterion values of all of the sub-echoes are estimated, and the sub-echo with the largest η value is selected as the velocity estimation object. The velocity estimated from the selected sub-echo is regarded as the current layer velocity.

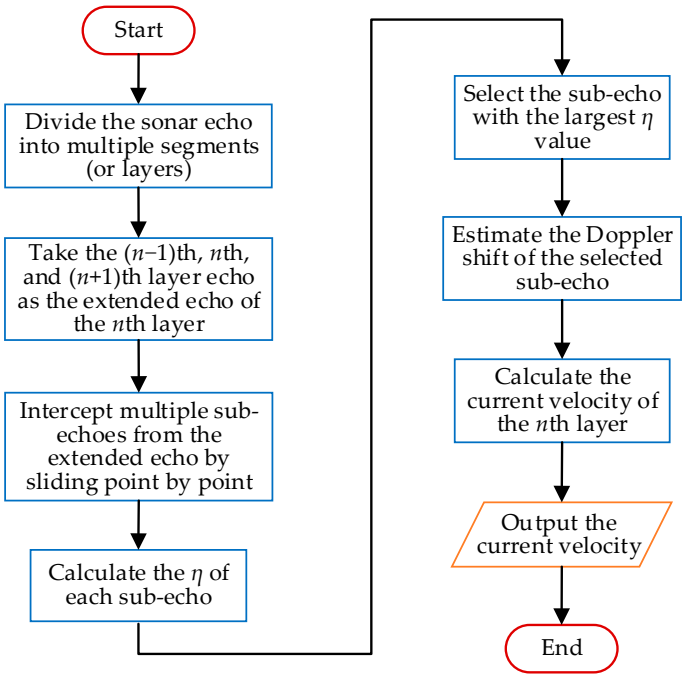

Figure 2. Flowchart of the accuracy selection method.

3. Prototype Experiment

In order to verify the estimation bias and accuracy of the proposed velocity estimation method, a water tank experiment and two field experiments were conducted with a prototype Doppler sonar system, and are detailed in this section. In Section 3.1, the implementation of these three experiments is described in detail. The results and analyses of the water tank experiment and the field experiments are illustrated in Sections 3.2–3.4, respectively.

3.1. Experiment Implementation

In order to test the estimation bias of the proposed velocity estimation method, a water tank experiment was conducted using a prototype Doppler sonar system in the laboratory. Since the walls and the bottom of the tank were equipped with sound-absorbing materials, the backscattering of the inclined sound beam was very weak. We fixed the Doppler sonar device horizontally on a bracket near the south wall of the tank, and made the fourth beam illuminate the opposite tank wall vertically. The advantage of this arrangement was that at least one beam could have a strong reflection echo. In order to verify the bias of the proposed method, three methods were used to estimate the bottom velocity: the proposed method in this paper, the MF method, and the WT method. In the tank experiment, we only compared the velocity estimation performance of the three methods for the fourth beam's echo. The top-view schematic diagram of the experimental tank is shown in Figure 3a, and the photograph of the sonar prototype and the tank is shown in Figure 3b.

In order to verify the accuracy (suppression capability for random errors) of the proposed velocity estimation method, field experiments were conducted with a prototype Doppler sonar device in the Shitoucheng section of the Qinhuai River in Nanjing. The map of the experimental river section is shown in Figure 4a, where the orange dotted line represents the course of the survey ship. The experimental river section is about 1.5 km long, with a surface width of about 60 m, and an average depth of about 5.5 m. The survey ship was a catamaran garbage scavenger, equipped with a fuel engine. It was about 4 m in length and 2 m wide. Catamarans are more stable than other boats, and it is easy to install and fix instruments on them. The field photo of the experiment is shown in Figure 4b. During the experiment, the prototype was located in the middle of the bow, and was fixed in place by fixtures and ropes.

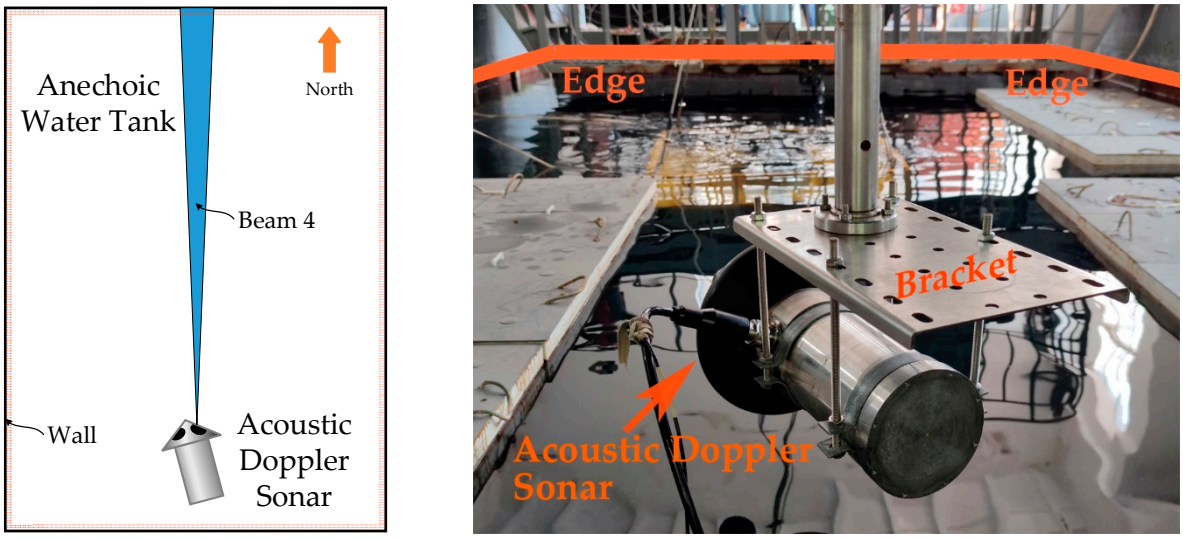

(a) (b)

Figure 3. Implementation of the anechoic tank experiment: (**a**) the top view of the anechoic tank; (**b**) the installation and fixation of the sonar prototype.

(a) (b)

Figure 4. (**a**) Map of the experimental river section and (**b**) photo of the field experiment implementation.

The Doppler sonar prototype uses the broadband measurement method, and the transmitted signal is a phase-encoded pulse. The prototype can measure the current velocity in real time and store the original echo data for post-processing. Other parameters of the prototype are shown in Table 2.

The field experiment was divided into two projects: a static ship experiment, and a moving ship experiment. In the static ship experiment, the ship was anchored in the middle of the river, and the theoretical relative velocity between the bottom and the prototype was zero. In the moving experiment, the ship sailed along the river's centerline as shown by the dotted line in Figure 4a, and the ship's velocity was maintained at about 2 m/s. In order to verify the performance of the proposed method, three methods were used to estimate the bottom velocity: the proposed method in this paper, the MF method, and the WT method. Then, the velocity standard deviations of the three methods were compared, since the current velocity changed constantly, introducing additional uncertainty into the

velocity estimations. Because the bottom is static relative to the earth, the bottom velocity is more stable than the current velocity. Therefore, the bottom velocity was chosen as the comparison parameter, which can highlight the performance differences between the signal processing methods. In the same way, this paper only compares the radial velocity estimation performance of one beam, in order to avoid the uncertainty caused by the attitude sensor. The experimental results and analysis are detailed below.

Table 2. The main parameters of the experimental prototype.

Serial Number	Parameters	Values
1	Carrier frequency	600 kHz
2	System bandwidth	50 kHz
3	Minimum layer thickness	0.1 m
4	Velocity estimation resolution	0.5 mm/s
5	Number of beam	4
6	Beam spreading	3 degrees
7	Beam angle	30 degrees
8	Velocity measurement range	±5 m/s
9	Maximum profiling distance	60 m
10	Maximum depth	100 m

3.2. Water Tank Experiment

The echo samples collected by the fourth Doppler sonar beam in a single transmission are shown in Figure 5a, where the figures above and below are a pair of orthogonal waveforms obtained after the down-conversion. The total signal duration was 20 ms, the bottom echo arrived at around 9.15 ms, and the corresponding range was about 6.9 m. In Figure 5a, the bottom echo is shown in the red dashed box, which is enlarged and shown in Figure 5b. The envelope of the phase-encoded signal can be clearly observed from Figure 5b.

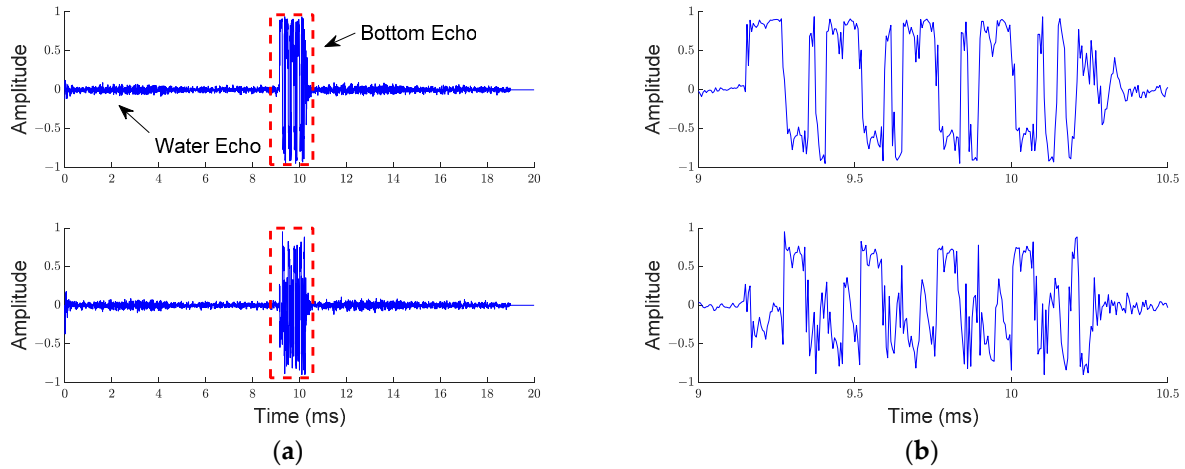

Figure 5. One-beam echo of the sonar prototype in the water tank experiment: (**a**) a pair of orthogonal down-conversion echoes; (**b**) the enlarged bottom echoes.

The proposed method, the MF method, and the WT method were used to estimate the bottom velocity of the fourth beam. Figure 6 shows the bottom velocity estimation results, with 100 sample points. The black, blue, and red curves represent the estimation results of the MF method, the WT method, and the proposed method, respectively. Three average velocity estimations are all close to zero, whereas the fluctuation ranges of the MF method and the WT method are clearly larger than that of the proposed method. Table 3 lists the mean values and the standard deviations of the bottom velocity estimations of the three methods, among which the mean velocity of the proposed method is closest to

the actual velocity, and its standard deviation is the least. Compared with the MF method, the bias and the standard deviation of the proposed method were reduced on average by 86% and 91%, respectively. Compared with the WT method, the bias and the standard deviation of the proposed method were reduced on average by 97% and 89%, respectively. Compared with the other two methods, the mean velocity was closer to the actual velocity, which indicates that the estimation error of the proposed method is smaller, while the lesser standard deviation demonstrates that the accuracy of the proposed method is higher.

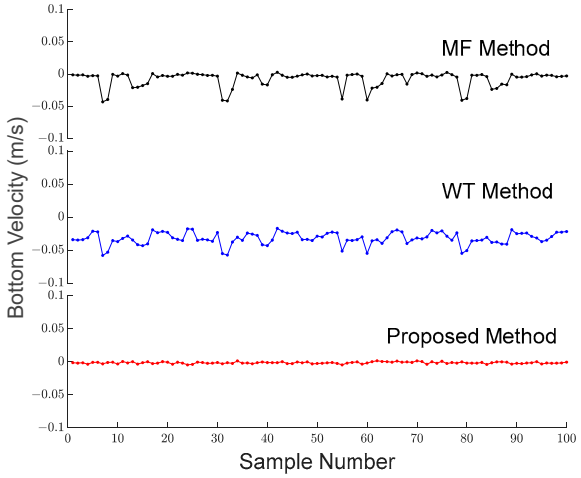

Figure 6. Bottom velocity estimation results of the three methods in the water tank experiment.

Table 3. Bottom velocity estimation performance of the three methods in the water tank experiment.

	MF Method	WT Method	Proposed Method
Mean velocity (m/s)	−0.007	−0.032	0.001
Velocity standard deviation (m/s)	0.011	0.009	0.001

3.3. Static Ship Experiment

In the static ship experiment, the survey ship was anchored and stationary in the middle of the channel. The ship was kept as static as possible, and the theoretical velocity of the prototype relative to the bottom was zero. However, due to the influence of the wind and the current, the Doppler sonar device still wobbled significantly, which increased the velocity estimation variance. The echo samples collected by the fourth Doppler sonar beam in a single transmission are shown in Figure 7a, where the figures above and below are a pair of orthogonal waveforms obtained after the down-conversion. The total signal duration was 20 ms, the bottom echo arrived at around 4 ms, and the corresponding water depth was about 2.6 m. In Figure 7a, the bottom echo is shown in the red dashed box, which is enlarged and shown in Figure 7b. It can be clearly observed from Figure 7b that the repetition number of the phase-encoded signal is 4, and the transmitted pulse width is about 0.6 ms.

The proposed method, the MF method, and the WT method were used to estimate the bottom velocities of the four beams. Figure 5 shows the bottom velocity estimation results of the four beams, with 100 sample points in each beam. Figure 8a–d corresponds to the first to the fourth beams, respectively. The black, blue, and red curves represent the estimation results of the MF method, the WT method, and the proposed method, respectively. Three average velocity estimations are all close to zero, whereas the fluctuation range of the MF method is clearly larger than that of the other two methods. The fluctuation range of the waveform-tracking method is close to that of the proposed method, but the statistical data show the better accuracy of the proposed method. Table 4 lists the mean values and the standard deviations of the bottom velocity estimations of the three methods, among which

the standard deviation of the proposed method is the least. Compared with the MF method, the velocity standard deviation of the proposed method was reduced by 50% on average, and the maximum reduction of a single beam's velocity standard deviation was 60%. Compared with the WT method, the velocity standard deviation of the proposed method was reduced by 20% on average, and the maximum reduction of a single beam's velocity standard deviation was 27%. The experimental results demonstrate that the accuracy of the proposed method is superior to that of the others. Table 3 also compares the calculation times of the three methods for single bottom velocity estimation, using MATLAB 2018b. The calculation times of the proposed method, the WT method, and the MF method were 3.26 ms, 2.2 ms, and 0.47 ms, respectively. The calculation time of the proposed method increased slightly, but the effect on the data update rate of the Doppler sonar system was negligible.

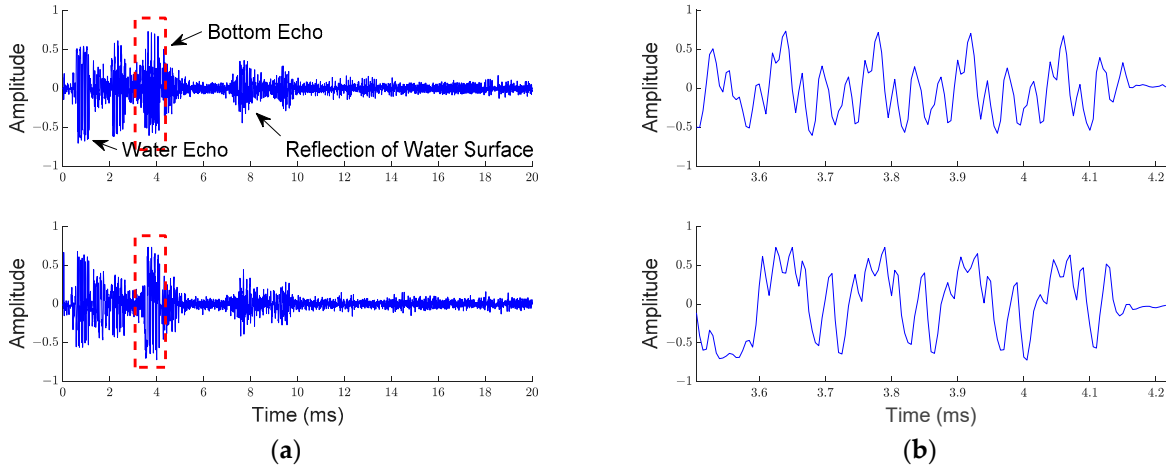

Figure 7. One-beam echo of the sonar prototype in the static ship experiment: (**a**) a pair of orthogonal down-conversion echoes; (**b**) the enlarged bottom echoes.

Table 4. Bottom velocity estimation performance of the three methods in the static ship experiment.

	Beam	MF Method	WT Method	Proposed Method
Mean velocity (m/s)	1	0.053	0.034	0.027
	2	0.021	0.019	0.027
	3	0.037	0.045	0.053
	4	0.063	0.047	0.044
Velocity standard deviation (m/s)	1	0.109	0.049	0.044
	2	0.154	0.108	0.084
	3	0.142	0.093	0.074
	4	0.082	0.059	0.043
Calculation time (ms)		0.47	2.20	3.26

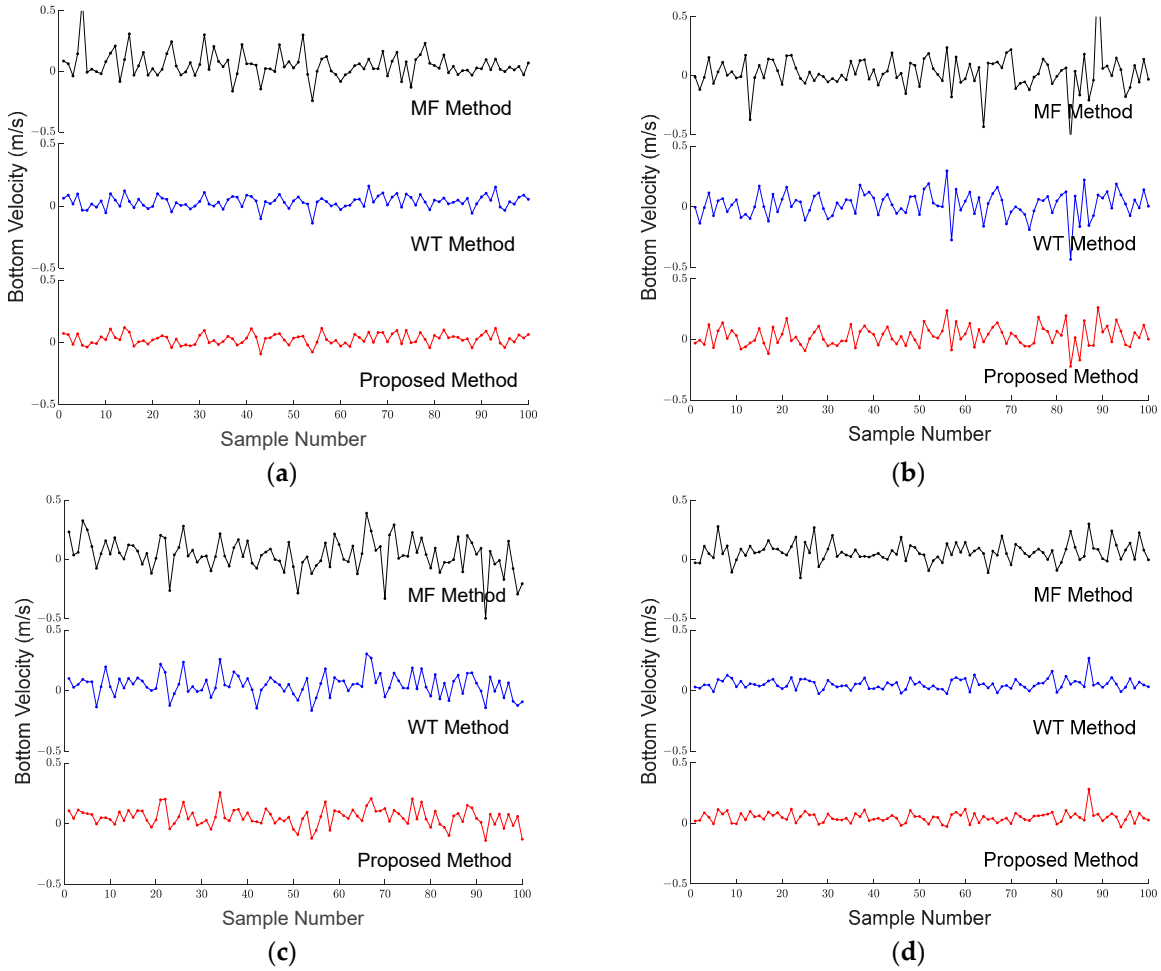

Figure 8. Bottom velocity estimation results of the three methods in the static ship experiment: (**a**) beam 1; (**b**) beam 2; (**c**) beam 3; (**d**) beam 4.

3.4. Moving Ship Experiment

In the moving ship experiment, the ship sailed along the river's centerline at a constant speed. The positional relationship of the four Doppler sonar beams is shown in Figure 9, and the arrow points in the direction of the survey ship. Beam 1 was aimed in the same direction as the ship, and its theoretical radial velocity was estimated to be about 1 m/s based on the ship's velocity. Beam 3 was aimed in the opposite direction to the ship, and its theoretical radial velocity was estimated to be about −1 m/s based on the ship's velocity. Beam 2 and beam 4 were aimed perpendicular to the sailing direction of the ship, so their theoretical radial velocity was zero.

The echo samples collected by the third Doppler sonar beam in a single transmission are shown in Figure 10a, where the figures above and below are a pair of orthogonal waveforms obtained after the down-conversion. The total signal duration was 20 ms, the bottom echo arrived at around 8 ms, and the corresponding water depth was about 5.5 m. In Figure 10a, the bottom echo is shown in the red dashed box, which is enlarged and shown in Figure 10b. As can be seen from Figure 10b, the bottom echo becomes disorderly and the repetition times of the phase-encoded signal cannot be distinguished. This is mainly because the bottom echo of beam 3 had a Doppler frequency shift of several hundred Hertz when the ship was moving. In Figure 10b, the bottom echo is broadened significantly, and the transition zone is much wider than in the static ship experiment. The transmitted pulse width was about 0.6 ms in this experiment, while the bottom echo width was more than 1.4 ms, as shown in Figure 10b. For the velocity measurement method based on the threshold judgment, the transition zone may be included in the bottom echo, which

will definitely increase the estimation error. Although the velocity measurement method based on the WT method can eliminate the transition zone, the amplitude and width of the transition zone are usually very different from the theoretical estimation. The method in this paper improves the estimation accuracy by tracking the echo segment with the smallest velocity estimation deviation, which compensates significantly for the shortcomings of existing methods.

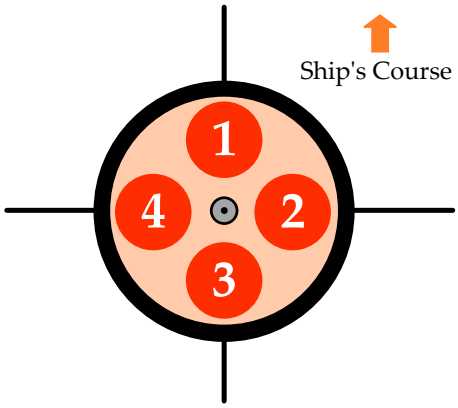

Figure 9. The positional relationship of the four beams of the sonar prototype.

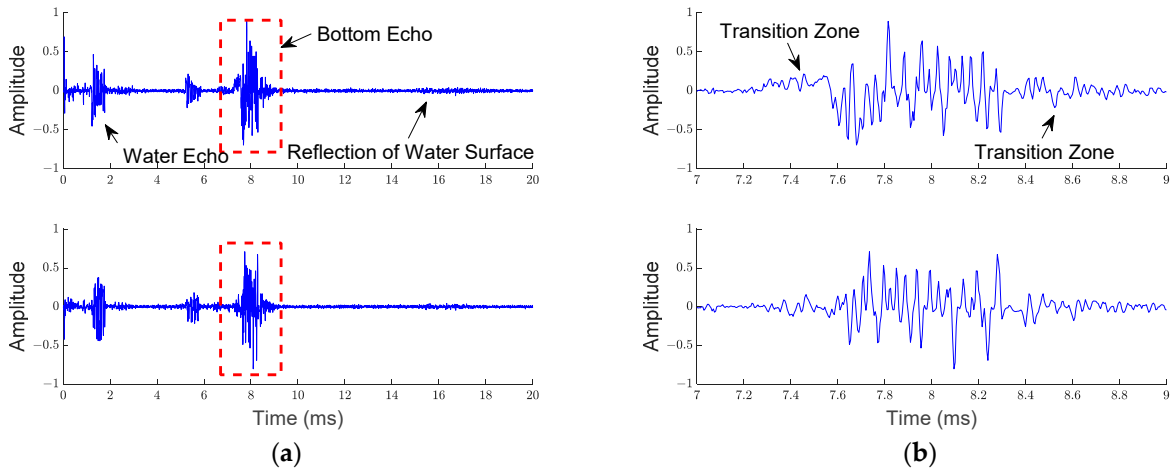

Figure 10. One-beam echo of the sonar prototype in the moving ship experiment: (**a**) a pair of orthogonal down-conversion echoes; (**b**) the enlarged bottom echoes.

The proposed method, the MF method, and the WT method were used to estimate the bottom velocities of the four beams. Figure 8 shows the bottom velocity estimation results of four beams, with 100 sample points in each beam. Figure 11a–d corresponds to the first to the fourth beams, respectively. The front and rear parts of the 1st and the 3rd beams made a difference to the mean velocities, due to the velocity change of the survey ship when it changed direction near the 50th sample point. The mean velocity estimated by the three methods was approximately equal to the theoretical value, but the fluctuation range of the proposed method was noticeably smaller than that of the others. Table 5 lists the mean values and the standard deviations of the bottom velocity estimations of the three methods, among which the standard deviation of the proposed method is the least. Compared with the MF method, the velocity estimation standard deviation of the proposed method decreased by 47% on average, and the maximum reduction of a single beam's velocity standard deviation was 67%. Compared with the wave-tracking method, the velocity estimation standard deviation of the proposed method was reduced by 33% on average, and the maximum reduction of a single beam's velocity standard deviation

was 57%. The experimental results demonstrate that the accuracy of the proposed method is superior to that of the other two methods. The calculation times of the three methods for single bottom velocity estimation are compared in Table 4. The calculation times of the proposed method, the WT method, and the MF method were 3.29 ms, 0.96 ms, and 0.47 ms, respectively. Similarly to the static ship experiment, the increased calculation time of the proposed method hardly affected the data update rate of Doppler sonar system.

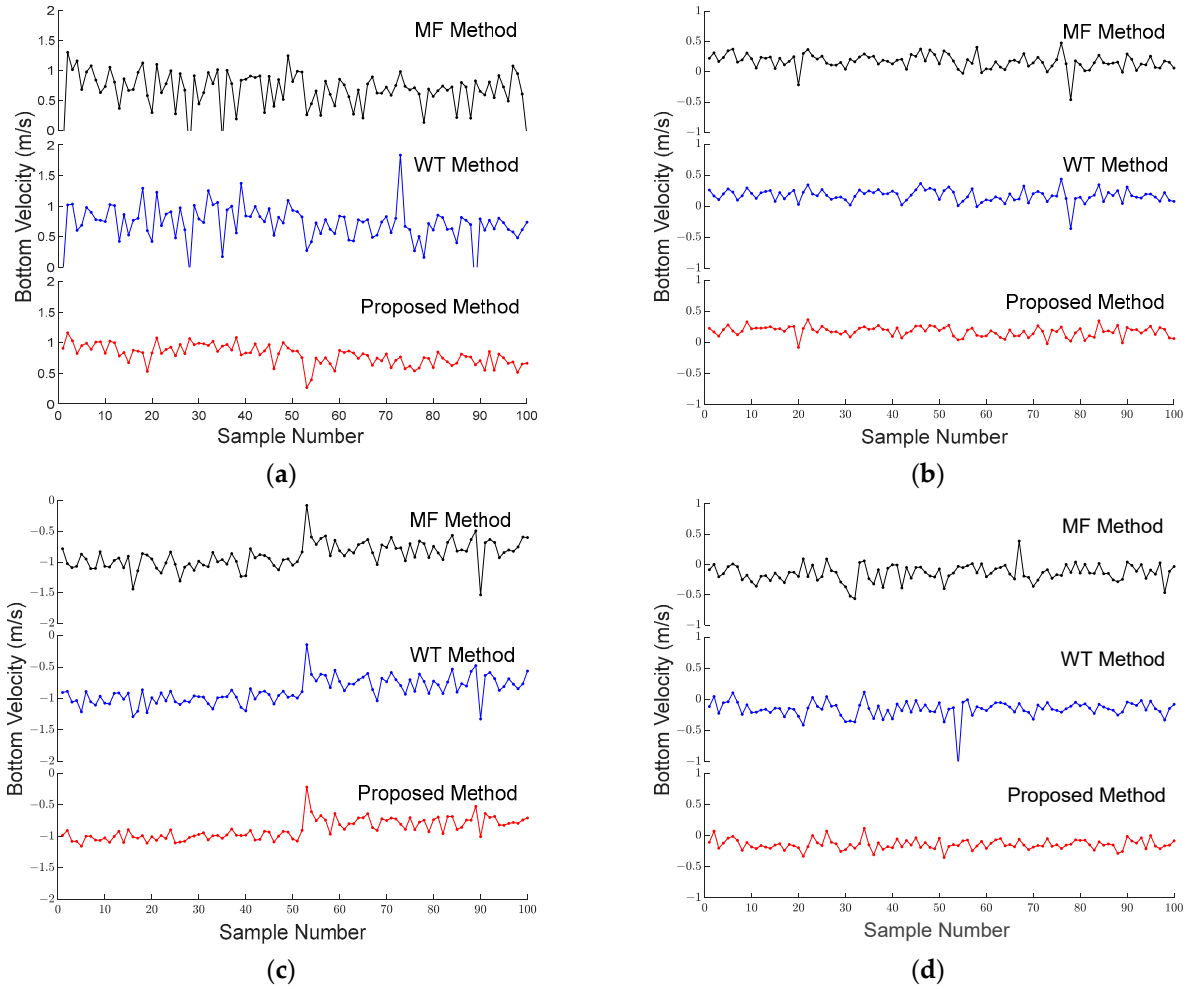

Figure 11. Bottom velocity estimation results of the three methods in the moving ship experiment: (**a**) beam 1; (**b**) beam 2; (**c**) beam 3; (**d**) beam 4.

Table 5. Bottom velocity estimation performance of the three methods in the moving ship experiment.

	Beam	MF Method	WT Method	Proposed Method
Mean velocity (m/s)	1	0.735	0.815	0.903
	2	0.203	0.194	0.201
	3	−1.012	−1.006	−1.006
	4	−0.162	−0.151	−0.137
Velocity standard deviation (m/s)	1	0.363	0.281	0.120
	2	0.105	0.078	0.071
	3	0.133	0.101	0.066
	4	0.146	0.131	0.090
Calculation time (ms)		0.47	0.96	3.29

4. Conclusions

A velocity estimation method based on accuracy evaluation and selection for Doppler sonar was proposed in this paper, in order to resolve the defects in accurate velocity estimation via the matched filtering method or the waveform-tracking method.

In the novel method, the Doppler sonar echo is divided into several segments with the same width as the transmitted pulse, and each segment reflects the information of its corresponding water layer. It was found that the velocity estimation accuracy of the segment was positively correlated with the ratio of its autocorrelation modulus to its power. According to this finding, we designed a criterion value in order to evaluate the accuracy of velocity estimation, with which the optimal velocity estimation values for water layers or bottoms can be obtained by selecting the segment with the highest criterion value. The η criterion value can be figured out with low calculation complexity and high reliability. The proposed accuracy selection method flexibly selects the echo interval in the processing based on the criterion value, so as to maintain optimal performance for current or bottom velocity estimation.

A water tank experiment was conducted using a prototype Doppler sonar device in order to verify the bias of the proposed method. Compared with the MF method and the WT method, the average velocity estimation bias of the proposed method was reduced by about 91% and 89%, respectively, in the water tank experiment.

Two field experiments were conducted using a prototype Doppler sonar device in order to verify the accuracy of the method—namely, the static and moving ship experiments. Compared with the matched filter method and the waveform-tracking method, the average velocity estimation deviation of the proposed method was reduced by about 50% and 20%, respectively, in the static ship experiment, and 47% and 33%, respectively, in the moving ship experiment. The experimental results demonstrate that the proposed method is more accurate and more effective.

Author Contributions: Y.Y. designed the optimization methods, conducted the experiments, and wrote the draft of the manuscript. S.F. verified the optimization methods, and reviewed and edited the manuscript. All authors have read and agreed to the published version of the manuscript.

Funding: This research was funded in part by the Fundamental Research Funds for the Central Universities under Grant 2242021k30019; and in part by the National Natural Science Foundation of China under Grant 91938203, Grant 11704069, and Grant 11604048.

Institutional Review Board Statement: Not applicable.

Informed Consent Statement: Not applicable.

Data Availability Statement: Not applicable.

Acknowledgments: We would like to thank Cuicui Zhou, Zhaowen Sun, Fan Yang, JiuLong Yang, Lewen Tao, and Shuxia Huang for their help during the experiment.

Conflicts of Interest: The authors declare no conflict of interest.

References

1. Velasco, D.W.; Ogle, M.; Leung, P. Long range current measurement from a surface buoy in the Gulf of Mexico. In Proceedings of the OCEANS 2019 MTS/IEEE SEATTLE, Seattle, WA, USA, 27–31 October 2019; pp. 1–10.
2. Sirabahenda, Z.; St-Hilaire, A.; Courtenay, S.C.; Van Den Heuvel, M.R. Comparison of acoustic to optical backscatter continuous measurements of suspended sediment concentrations and their characterization in an agriculturally impacted river. *Water* **2019**, *11*, 981. [CrossRef]
3. Thomas, L.P.; Marino, B.M.; Szupiany, R.N. Application of the two-ADCP technique in estuaries to characterize the suspended particulate matter transport. In Proceedings of the 2017 IEEE/OES Acoustics in Underwater Geosciences Symposium (RIO Acoustics), Rio de Janeiro, Brazil, 25–27 July 2017; pp. 1–5.
4. Cusi, S.; Rodriguez, P.; Pujol, N.; Pairaud, I.; Nogueras, M.; Antonijuan, J. Evaluation of AUV-borne ADCP measurements in different navigation modes. In Proceedings of the OCEANS 2017–Aberdeen, Aberdeen, UK, 19–22 June 2017; pp. 1–8.
5. Theriault, K. Incoherent multibeam Doppler current profiler performance: Part I—Estimate variance. *IEEE J. Ocean. Eng.* **1986**, *11*, 7–15. [CrossRef]

6. Zedel, L. Modeling pulse-to-pulse coherent Doppler sonar. *J. Atmos. Ocean. Technol.* **2008**, *25*, 1834–1844. [CrossRef]
7. Ivić, I.R. Effects of phase coding on Doppler spectra in PPAR weather radar. *IEEE Trans. Geosci. Remote Sens.* **2018**, *56*, 2043–2065. [CrossRef]
8. Dillon, J.; Zedel, L.; Hay, A.E. On the distribution of velocity measurements from pulse-to-pulse coherent Doppler sonar. *IEEE J. Ocean. Eng.* **2012**, *37*, 613–625. [CrossRef]
9. Chi, C.; Vishnu, H.; Beng, K.T.; Chitre, M. Robust resolution of velocity ambiguity for multifrequency pulse-to-pulse coherent Doppler sonars. *IEEE J. Ocean. Eng.* **2019**, *45*, 1506–1515. [CrossRef]
10. Brumley, B.H.; Cabrera, R.G.; Deines, K.L.; Terray, E.A. Performance of a broad-band acoustic Doppler current profiler. *IEEE J. Ocean. Eng.* **1991**, *16*, 402–407. [CrossRef]
11. Pinkel, R.; Smith, J.A. Repeat-sequence coding for improved precision of Doppler sonar and sodar. *J. Atmos. Ocean. Technol.* **1992**, *9*, 149–163. [CrossRef]
12. Tong, J.; Xu, X.; Zhang, T.; Zhang, L.; Li, Y. Study on installation error analysis and calibration of acoustic transceiver array based on SINS/USBL integrated system. *IEEE Access* **2018**, *6*, 66923–66939.
13. Sun, J.; Wang, J.; Shi, Y.; Hu, F.; Wang, X.; Yu, J.; Zhang, A. Self-noise spectrum analysis and joint noise filtering for the sea-wing underwater glider based on experimental data. *IEEE Access* **2020**, *8*, 42960–42970. [CrossRef]
14. Koyama, S.; Okubo, K.; Tagawa, N. Performance comparison of signal coding method in acoustic sensing for occlusion area using super-directional sound source. In Proceedings of the 2019 IEEE International Ultrasonics Symposium (IUS), Glasgow, UK, 6–9 October 2019; pp. 603–606.
15. Wang, Z.; Huang, S.; Wang, S.; Wang, Q.; Zhao, W. Design of electromagnetic acoustic transducer for helical Lamb wave with concentrated beam. *IEEE Sens. J.* **2020**, *12*, 6305–6313. [CrossRef]
16. Chi, C.; Vishnu, H.; Beng, K.T.; Chitre, M. Utilizing orthogonal coprime signals for improving broadband acoustic Doppler current profilers. *IEEE J. Ocean. Eng.* **2019**, *45*, 1516–1526. [CrossRef]
17. Jia, T.; Ho, K.C.; Wang, H.; Shen, X. Localization of a moving object with sensors in motion by time delays and Doppler shifts. *IEEE Trans. Signal Process.* **2020**, *68*, 5824–5841. [CrossRef]
18. Huang, H. Estimating the calibration error-caused bias limit of moving-boat ADCP streamflow measurements. *J. Hydraul. Eng. ASCE* **2020**, *146*, 06020006. [CrossRef]
19. Despax, A.; Le Coz, J.; Hauet, A.; Mueller, D.S.; Engel, F.L.; Blanquart, B.; Oberg, K.A. Decomposition of uncertainty sources in acoustic Doppler current profiler streamflow measurements using repeated measures experiments. *Water Resour. Res.* **2019**, *55*, 7520–7540. [CrossRef]
20. Velasco, D.W.; Wilson, W.D.; Nylund, S.; Heitsenrether, R. Enhancing the accuracy of current profiles from surface buoy-mounted systems. In Proceedings of the 2018 OCEANS–MTS/IEEE Kobe Techno–Oceans (OTO), Kobe, Japan, 28–31 May 2018; pp. 1–6.
21. Velasco, D.W.; Nylund, S. Performance improvement for ADCPs on surface buoys. In Proceedings of the 2019 IEEE/OES Twelfth Current, Waves and Turbulence Measurement (CWTM), San Diego, CA, USA, 10–13 March 2019; pp. 1–6.
22. Cui, J.; Li, Z.; Li, Q. Strong scattering targets separation based on fractional Fourier transformation in pulse-to-pulse coherent acoustical Doppler current profilers. *IEEE J. Ocean. Eng.* **2018**, *44*, 466–481. [CrossRef]
23. Prieur, F.; Hansen, R.E. Theoretical improvements when using the second harmonic signal in acoustic Doppler current profilers. *IEEE J. Ocean. Eng.* **2012**, *38*, 275–284. [CrossRef]
24. Chi, C.; Li, Z.; Li, Q. Design of optimal multiple phase-coded signals for broadband acoustical Doppler current profiler. *IEEE J. Ocean. Eng.* **2015**, *41*, 302–317.
25. Lin, Y.; Yuan, F.; Cheng, E. Using orthogonal combined signals in broadband ADCP for improving velocity measurement. *J. Mar. Sci. Eng.* **2020**, *8*, 450. [CrossRef]
26. Murray, J.J. On the Doppler bias of hyperbolic frequency modulation matched filter time of arrival estimates. *IEEE J. Ocean. Eng.* **2018**, *44*, 446–450. [CrossRef]